Testing Seismic Models of Hot B Subdwarfs with *Gaia* Data

G. Fontaine[1], P. Bergeron[1] , P. Brassard[1], S. Charpinet[2], S. Randall[3], V. Van Grootel[4], M. Latour[5] , and E. M. Green[6]

[1] Département de Physique, Université de Montréal, Montréal, QC H3C 3J7, Canada
[2] CNRS, Université de Toulouse, UPS-OMP, Toulouse, France
[3] ESO, Karl-Schwarzschild-Str. 2, D-85758 Garching bei München, Germany
[4] Space Sciences, Technologies and Astrophysics Research (STAR) Institute, Université de Liège, 19C Allée du 6 Août, B-4000 Liège, Belgium
[5] Institute for Astrophysics, Georg-August-University, Friedrich-Hund-Platz 1, D-37077 Göttingen, Germany
[6] Steward Observatory, University of Arizona, 933 North Cherry Avenue, Tucson, AZ 85721, USA

Abstract

We report the results of a study designed to test further the basic validity of the seismic models of hot pulsating B subdwarfs that have been developed over the last two decades. Given estimates of the effective temperature, surface gravity, and mass as obtained from a seismic analysis, and given an estimate of the He/H ratio as available from independent spectroscopy, it is possible to compute a "seismic distance" that is suitably corrected for interstellar reddening from a model atmosphere calculation in conjunction with two-band photometry. The test consists of comparing such a distance with that obtained directly from the high-accuracy *Gaia* parallax measurements that have become available through Data Release 2. Using observed magnitudes in the *Gaia* G_{BP}, G_{RP} bandpasses as well as ground-based photometry in the Johnson *B*, *V*, Strömgren *b*, *y*, and SDSS *g*, *r* filters, we find that all of our seismic estimates fall within 1σ of their parallax counterparts. In addition, the derived reddening for our target stars is shown to be generally consistent with Galactic dust reddening and extinction maps. These results apply to a sample of 14 pulsating hot B subdwarfs for which seismic models were published in the past. We also derive useful constraints on the distances to two more pulsators that belong to unresolved binary systems. The excellent agreement found between seismic and parallax distances for the bulk of the sample adds further credibility to the seismic models that have been calculated for pulsators of this type.

Key words: stars: atmospheres – stars: oscillations – subdwarfs

1. Introduction

Among the many types of pulsating stars currently known, pulsating hot B subdwarf (sdB) stars have turned out to be exceptional asteroseismological laboratories. There are two main families of pulsating sdBs, the short-period *p*-mode pulsators of the V361 Hya type discovered in 1997 (Kilkenny et al. 1997) and the cooler, less compact long-period *g*-mode oscillators of the V1093 Her type discovered in 2003 (Green et al. 2003). A few objects, lying mostly at the boundary between the two instability regions in the surface gravity-effective temperature domain, show both *p*- and *g*-mode pulsations and are referred to as hybrid pulsators (e.g., Baran et al. 2005; Schuh et al. 2006). These two categories of pulsators show strong analogies with the β Cephei/slowly pulsating blue stars on the main sequence (Fontaine et al. 2003). However, sdB stars lie well below the main sequence in the Hertzsprung–Russell diagram on the extreme horizontal branch and are hot ($22{,}000\,\mathrm{K} \lesssim T_{\mathrm{eff}} \lesssim 42{,}000\,\mathrm{K}$), compact ($5.2 \lesssim \log g \lesssim 6.2$) core helium burning objects. Their overall properties and evolutionary status were last reviewed by Heber (2016).

Since the discovery that a significant fraction of sdB stars pulsate, tremendous progress has been made in terms of exploiting their asteroseismological potential (see, e.g., Charpinet et al. 2016 for a recent review). In particular, Brassard et al. (2001) first adapted the forward asteroseismological approach to sdB pulsators using parameterized static models of these stars. In this method, a detailed search in parameter space is carried out with the aim of finding an optimal model whose computed pulsation periods best match the observed periods. The technique was then vastly improved over the years with the

development of sophisticated optimization tools and new generations of stellar models. For *p*-mode pulsators, which can be well studied from the ground due to their relatively short periods of a few minutes and their amplitudes of several millimags, asteroseismic studies of the sort have led, typically, to the determination of fundamental parameters such as the total mass, the surface gravity, the effective temperature, and the mass of the H-rich envelope (e.g., Charpinet et al. 2005c; Van Grootel et al. 2013). In some cases inferences about the internal rotation profile could be obtained (e.g., Charpinet et al. 2008). Furthermore, on the basis of such studies, a first view of the empirical mass distribution of sdB stars was provided by Fontaine et al. (2012).

For their part, the *g*-mode pulsators remained difficult to study from the ground due to their much longer observed periods, from ∼0.5 to ∼4 hr, and their small amplitudes of typically less than 1 mmag (e.g., Randall et al. 2006b, 2006c). It thus took the advent of space-borne observations to exploit the additional seismic riches associated with *g*-modes, which probe much deeper inside sdB stars than *p*-modes do. The first attempt to derive the fundamental parameters, as well as to probe the core of an sdB pulsator, was made by Van Grootel et al. (2010b) for the *g*-mode pulsator KPD 0629−0016 on the basis of *CoRoT* data (Charpinet et al. 2010). This was followed by the study of Van Grootel et al. (2010a) and Charpinet et al. (2011) on the *g*-mode pulsators KPD 1943+4058 and KIC 02697388, respectively, using *Kepler* observations. These investigations led to the strong suggestion that the convective mixed core in sdB stars is significantly larger than expected from standard evolutionary models, thus demonstrating the potential of these stars for investigating the structure and evolution of core helium burning objects. Most recently,

Charpinet et al. (2019) used *Transiting Exoplanet Survey Satellite* (*TESS*) data to model the newly discovered *g*-mode pulsator TIC 278659026, and reached similar conclusions.

To date, a total of 16 pulsating sdB stars (12 *p*-mode and 4 *g*-mode variables) have been modeled through the approach pioneered by Brassard et al. (2001). We note that, in most cases, the values of the surface gravity log *g* and of the effective temperature T_{eff} inferred from seismology have been tested against independent measurements obtained through standard quantitative analyses of the time-averaged optical spectrum of a target star. This compatibility with spectroscopy was deemed a necessary condition for searching for, and ultimately accepting, a seismic solution in all but one of these investigations.[7] It has been an inherent part of the whole approach from the very beginning, and constitutes a fundamental test.

The recent release (DR2) of high-accuracy parallax measurements from *Gaia* (Gaia Collaboration et al. 2018) provides another opportunity for testing independently the available seismic models for pulsating sdB stars. Indeed, it is possible to obtain an independent estimate of the distance to a given pulsator by computing a model atmosphere and a synthetic spectrum specified by the seismic values of the surface gravity, effective temperature, and mass (or radius), three of the fundamental properties that routinely come out of such seismic exercises.[8] This allows for the computation of an absolute magnitude in a given bandpass, which, combined with an observed magnitude, leads to a "seismic distance." This estimate can be refined by taking into account interstellar reddening, since the latter cannot be ignored for these sdB stars typically located at distances of ∼1 kpc. This requires minimally two-band photometry. The test then consists in comparing the seismic distance with that obtained directly from the *Gaia* parallax for a given pulsator. A weaker component of the test is to verify if the inferred value of the reddening index, $E(B-V)$, is also compatible with line-of-sight measurements as provided by Galactic dust reddening and extinction maps. The index $E(B-V)$, which measures extinction between Earth and a given star, is deemed acceptable if it is smaller than (or equal to) the total extinction along the line of sight.

In this paper, we consider the 16 pulsating sdB stars for which detailed seismic models have been derived so far. As is clear from Charpinet et al. (2019) for example, the parameterized forward modeling approach put forward initially by Brassard et al. (2001) has now become a powerful tool for extracting the seismic information contained in the observed pulsation periods of a star. In this rising era of *TESS*, which is providing tens of new light curves for pulsating sdB stars, the method will find many more applications. In this context, we felt that, with the recent availability of *Gaia* DR2 data, we could not miss the opportunity to further test it.

2. Available Data

2.1. Basic Properties of the Seismic Models

Table 1 identifies each of the 16 pulsating sdB stars of interest, along with their seismically determined values of the surface gravity, effective temperature, and total mass as provided in the original analysis papers listed as references.[9] The quoted uncertainties in the table are the formal errors of the seismic fit in parameter space and do not include possible systematic errors, which remain very difficult to estimate. We note that 4 of the stars listed in Table 1 are *g*-mode pulsators (KPD 1943+4058, KPD 0629−0016, KIC 02697388, and TIC 278659026), while the 12 others are *p*-mode pulsators. We note further that in the seismic studies carried out on Feige 48 (Charpinet et al. 2005b), PG 1325+101 (Charpinet et al. 2006b), PG 0911+456 (Randall et al. 2007), and EC 09582 −1137 (Randall et al. 2009), the effective temperature was fixed a priori at the value inferred from spectroscopy. This is because only a few pulsation periods (acting as constraints) were available in those four cases, and fixing the effective temperature provided a welcome additional constraint in searching for a seismic solution in parameter space. The choice of that parameter over others was motivated by the observation that the mechanical structure of a typical sdB star is such that the pulsation periods are much more sensitive, in a relative sense, to a variation of surface gravity than to a variation of the effective temperature (see, e.g., Charpinet 1999). Spectroscopy can provide more precise values of T_{eff} than asteroseismology for sdB stars, while the converse is true for log *g* (Brassard et al. 2001).

It should be pointed out that the target stars chosen in most of the seismic analyses summarized in Table 1 were selected on the basis of their simplicity and stability as pulsators, as well as their brightness. In addition, a conscious effort was made to avoid, if possible, targets with light curves and spectra contaminated by the flux of a companion in unresolved binary systems. In this way, the sample is biased against binarity, which is a frequent phenomenon in sdB stars (see, e.g., Heber 2016). For the specific purpose of seismic modeling, all but one of the stars listed in Table 1 can be considered as isolated. The exception is PG 1336−018, which is a close eclipsing binary system made of a pulsating sdB component and an M dwarf companion (Kilkenny et al. 1998). This is a spin–orbit synchronized system with a period of 2.4244 hr, and is the only case where terms higher than first-order in rotation and tidal interaction had to be taken into account in the seismic modeling itself (see Charpinet et al. 2008). Otherwise, the modeling exercise was carried out within the slow-rotation approximation for isolated stars.

2.2. Atmospheric Parameters from Quantitative Spectroscopy

Table 2 gives the atmospheric parameters of the 16 stars of interest as inferred from quantitative spectroscopy, independently of any seismic considerations. These are the surface gravity, the effective temperature, and the number ratio of helium-to-hydrogen in these H-dominated hot stars. The uncertainties given in the table are those quoted in the original references and correspond solely to the formal errors of the spectral fit. In most cases, the atmospheric analyses have been carried out in a homogeneous way, following the method developed by Bergeron et al. (1992)[10] and using (1) time-averaged optical spectra gathered by one of us (E.M.G.) at the

---

[7] The exception is the binary star PG 0048+091, for which a seismic model was proposed by Charpinet et al. (2006a) a few years before Østensen et al. (2010) deconvolved the polluted spectrum of the sdB component.

[8] Note that, to zeroth order, the atmospheric chemical composition for sdB stars is pure H, but see below.

[9] In the case of KIC 02697388, Charpinet et al. (2011) have provided two equally acceptable seismic models, which are very close to each other in parameter space.

[10] This is based on a χ^2 minimization procedure that relies on the method of Levenberg–Marquart. Normalized lines of both the observed and model spectra are thus compared, making the method largely free of flux calibration issues.

Table 1
Basic Characteristics of the Seismic Models

Name	log g (cm s^{-2})	T_{eff} (K)	M ($M_\odot$)	References
PG 1047+003	5.800 ± 0.006	33000 ± 1600	0.490 ± 0.014	Charpinet et al. (2003)
PG 0014+067	5.775 ± 0.009	33940 ± 3520	0.477 ± 0.024	Charpinet et al. (2005a)
PG 1219+534	5.807 ± 0.006	33640 ± 1360	0.457 ± 0.012	Charpinet et al. (2005c)
Feige 48	5.437 ± 0.006	29580 ± 370	0.460 ± 0.008	Charpinet et al. (2005b)
EC 05217−3914	5.730 ± 0.008	32000 ± 1800	0.490 ± 0.020	Billères & Fontaine (2005)
PG 1325+101	5.811 ± 0.004	35050 ± 220	0.499 ± 0.011	Charpinet et al. (2006b)
PG 0048+091	5.711 ± 0.010	33300 ± 1700	0.447 ± 0.027	Charpinet et al. (2006a)
EC 20117−4014	5.856 ± 0.008	34800 ± 2000	0.540 ± 0.040	Randall et al. (2006a)
PG 0911+456	5.777 ± 0.002	31940 ± 220	0.390 ± 0.010	Randall et al. (2007)
BAL 090100001	5.383 ± 0.004	28000 ± 1200	0.432 ± 0.015	Van Grootel et al. (2008)
EC 09582−1137	5.788 ± 0.004	34805 ± 230	0.485 ± 0.011	Randall et al. (2009)
KPD 1943+4058	5.520 ± 0.030	28050 ± 470	0.496 ± 0.002	Van Grootel et al. (2010a)
KPD 0629−0016	5.450 ± 0.034	26290 ± 530	0.471 ± 0.002	Van Grootel et al. (2010b)
KIC 02697388[a]	5.489 ± 0.033	25622 ± 420	0.463 ± 0.009	Charpinet et al. (2011)
KIC 02697388[b]	5.499 ± 0.049	25555 ± 520	0.452 ± 0.011	Charpinet et al. (2011)
PG 1336−018	5.775 ± 0.007	32850 ± 175	0.471 ± 0.006	Van Grootel et al. (2013)
TIC 278659026	5.572 ± 0.056	23738 ± 640	0.391 ± 0.013	Charpinet et al. (2019)

Notes.
[a] Seismic Model 1.
[b] Seismic Model 2.

Table 2
Spectroscopic Constraints

Name	log g (cm s^{-2})	T_{eff} (K)	log He/H	References
PG 1047+003	5.800 ± 0.040	33150 ± 200	−1.91 ± 0.02	Charpinet et al. (2003)
PG 0014+067	5.770 ± 0.046	34130 ± 370	−1.68 ± 0.03	Charpinet et al. (2005a)
PG 1219+534	5.810 ± 0.046	33600 ± 370	−1.49 ± 0.08	Charpinet et al. (2005c)
Feige 48	5.480 ± 0.046	29580 ± 370	−2.95 ± 0.08	Charpinet et al. (2005b)
EC 05217−3914	5.760 ± 0.060	31300 ± 220	⋯	Koen et al. (1999)
PG 1325+101	5.810 ± 0.040	35050 ± 220	−1.70 ± 0.02	Charpinet et al. (2006b)
PG 0048+091	5.69	34200	−3.0	Østensen et al. (2010)
EC 20117−4014	5.900 ± 0.060	34898 ± 260	⋯	O'Donoghue et al. (1997)
PG 0911+456	5.767 ± 0.029	31940 ± 220	−2.55 ± 0.06	Randall et al. (2007)
BAL 090100001	5.450 ± 0.030	28555 ± 217	−2.67 ± 0.03	Van Grootel et al. (2008)
EC 09582−1137	5.794 ± 0.044	34805 ± 230	−1.68 ± 0.06	Randall et al. (2009)
KPD 1943+4058	5.552 ± 0.041	27732 ± 269	−2.71 ± 0.16	Van Grootel et al. (2010a)
KPD 0629−0016	5.473 ± 0.027	26484 ± 196	−2.79 ± 0.04	Van Grootel et al. (2010b)
KIC 02697388	5.500 ± 0.031	25395 ± 227	−2.77 ± 0.12	Charpinet et al. (2011)
PG 1336−018	5.771 ± 0.015	32807 ± 82	−2.92 ± 0.09	Van Grootel et al. (2013)
TIC 278659026	5.650 ± 0.030	23720 ± 260	−3.22 ± 0.63	Németh et al. (2012)

Steward Observatory, and (2) grids of NLTE, metal-blanketed atmosphere models and synthetic spectra computed with the public codes TLUSTY and SYNSPEC at the Université de Montréal (see, e.g., Brassard et al. 2010). The exceptions are the southern hemisphere objects, EC 05217−3914 and EC 20117−4014, analyzed with pure H models, the binary system PG 0048+091, and the case of TIC 278659026 analyzed by Németh et al. (2012) using similar tools (TLUSTY/SYN-SPEC) as above.

At the beginning of this investigation, four stars in the sample were known to be part of unresolved binary systems. The other targets were not. In descending order in Table 2, Feige 48 was believed, until recently, to consist of a pulsating sdB star and an invisible white dwarf companion (O'Toole et al. 2004). Preliminary work by several of us at the Steward Observatory now indicates that the light curve of the Feige 48

system shows a very weak reflection effect, implying that the companion is rather a late type M dwarf (Latour et al. 2014a). Still, the latter has very little effect on the normalized optical line profiles of H and He used in the fitting procedure employed to derive the atmospheric parameters of the sdB component (see, e.g., Latour et al. 2014b). In contrast, the optical spectrum of PG 0048+091 is significantly polluted by the light of a G0–G2 main-sequence companion according to Koen et al. (2004). The amount of pollution is even higher in the EC 20117−4014 system due to the presence of an F5 dwarf star (O'Donoghue et al. 1997). In both cases, deconvolution procedures were needed to infer the atmospheric parameters of the pulsating sdB component. As a consequence, those estimates are more uncertain (Østensen et al. 2010). Finally, PG 1336−018 has also a much fainter M5 dwarf companion, according to Kilkenny et al. (1998), so the light pollution issue is much

reduced in this case, despite a significant reflection effect. Therefore, fitting its H and He spectral lines shortward of ~5000 Å gave reliable values of its atmospheric parameters (Charpinet et al. 2008).

2.3. Photometric Data

Table 3 provides a compilation of the available two-band photometry that we found in the literature. We used the *Gaia* Archive DR2 to extract, for each star of interest, the apparent magnitude G_{BP} (second column) and color index $(G_{BP} - G_{RP})$ (third column). This photometry from *Gaia* is both very accurate and homogeneous. Although generally less accurate, very good ground-based data exist for many of these relatively bright stars, and we found it interesting to investigate how the results would fare against each other. Hence, we extracted useful data for 13 stars in the standard Johnson system, *V* and $(B - V)$ (columns 4 and 5), for 8 stars in the Strömgren system, *y* and $(b - y)$ (columns 6 and 7), and 4 stars in the SDSS *ugriz* system, *g* and $(g - r)$ (columns 8 and 9). Altogether, we compiled magnitudes and color indices for 41 pairs.

Among other features, using the $(G_{BP} - G_{RP})$ index, we draw attention to the very red color measured in the binary systems PG 0048+091 and EC 20117−4014 compared to single stars of similar effective temperature. Of course, there is no surprise here, as both objects contain a main-sequence companion that contributes significantly to (in the case of the G0–G2 companion in PG 0048+09), and even dominates (in the case of the F5 companion in EC 20117−4014), the luminosity of the system in the optical domain as indicated above. Also, the $(G_{BP} - G_{RP})$ index of KPD 0629−0016 is quite red, although not as extreme in comparison, but, in this case, interstellar reddening is surely the culprit, as the star is not known to be binary and lies in the galactic plane.

For PG 0048+091 and EC 20117−4014 the optical colors appear to be hopelessly too contaminated to be useful, but additional information can be gathered about them. Indeed, O'Donoghue et al. (1997) estimated from their deconvolution process that the apparent visual magnitude of the sdB component in EC 20117−4014 is $V = 13.55 \pm 0.05$ (compared to a magnitude of $V = 12.47 \pm 0.01$ for the system). Combined with a seismic estimate of the absolute magnitude of the pulsator in the *V* band, $M_V = 4.48 \pm 0.14$, obtained as described below, allows us to derive an upper limit (uncorrected for interstellar reddening) on the seismic distance. In the case of PG 0048+091, we assume that the companion has a representative absolute magnitude of $M_V = 4.9$ for a G1V star. Coupled to a seismic value of $M_V = 4.40 \pm 0.12$ for the sdB component, this leads to an estimate of its apparent magnitude of $V \simeq 14.8$ (compared to a magnitude of $V = 14.26 \pm 0.02$ for the system). From those, an upper limit on the seismic distance can again be derived, as is done below.

We also searched the Two Micron All Sky Survey (2MASS) catalog, mostly through the $(J - H)$ index, for the IR signature of potential companions in all of our 16 target stars and, in particular, in the 12 objects not known to be binaries (and see Green et al. 2008). In this way, we uncovered an IR excess in PG 0014+067, highly suggestive of the presence of a cool companion. According to Østensen et al. (2010), the orbital period would have to be longer than a few days for this system (radial velocity variations have been searched for, but only for periods of days and less), but this is also the case for PG 0048+091 (the actual orbital period is not known, but is much
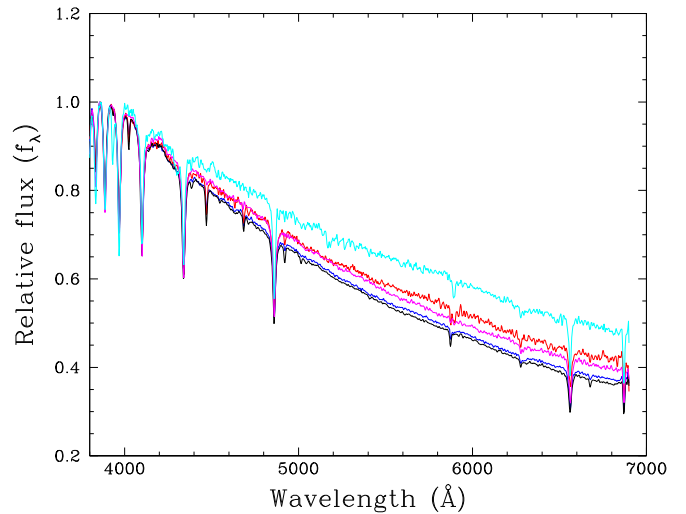

Figure 1. Comparison of the flux-calibrated, low-resolution spectra of PG 0048+091 (cyan), PG 0014+067 (red), PG 1336−018 (magenta), PG 1047+003 (blue), and PG 1219+534 (black). These data have been obtained with the Boller and Chivens Spectrograph attached to the Bok Telescope of the Steward Observatory. The claimed accuracy of the flux calibration is a few percent. These five pulsators all have similar estimates of T_{eff} and log *g* (see Table 2). PG 1047+003 and PG 1219+534 show no trace of binarity and can be considered as isolated stars. PG 0048+091 is known to be an unresolved binary containing an sdB and a G1 dwarf companion. Likewise, PG 1336−018 is also an unresolved binary, but contains a much fainter M5 dwarf companion displaying a strong reflection effect. Very likely, PG 0014+067 is also an unresolved binary system that contains a somewhat earlier dwarf than M5.

longer than several days according to Reed et al. 2019) and EC 20117−4014 (the orbital period has recently been determined to be 792.3 days by Otani et al. 2018).

In this context, we compare, in Figure 1, the carefully flux-calibrated spectra of five objects of interest, all with similar values of the effective temperature of the sdB component as given in Table 2. Our aim here is to illustrate the *slope* of these spectra, an exercise that should ideally be carried out for stars with the same values of log *g* and, particularly, T_{eff}. We picked two reference stars, PG 1047+003 ($T_{eff} = 33{,}150$ K) and PG 1219+534 ($T_{eff} = 33{,}600$ K), that can be considered as single as they show no IR excess and no radial velocity variations, at least on timescales of hours to days. We also picked the known binaries PG 1336−018 ($T_{eff} = 32{,}807$ K; M5V companion) and PG 0048+091 ($T_{eff} = 34{,}200$ K; G1V companion) to compare with the potential new binary PG 0014+067 ($T_{eff} = 34{,}130$ K). We do not have a similar spectrum for the southern hemisphere binary star EC 20117−4014 ($T_{eff} = 34{,}898$ K; F5V companion), and, at $T_{eff} = 29{,}580$ K, Feige 48 is too cool for proper comparison. What Figure 1 clearly shows is that the optical spectrum of PG 0014+067 is indeed polluted by the light of a companion, likely somewhat earlier than the M5 dwarf in the comparison system PG 1336−018. To our knowledge, this is the first time PG 0014+067 has revealed itself as an unresolved binary system. We thus retain 5 unresolved binary stars in our sample of 16 pulsators, and we anticipate consequences in our discussion below of interstellar versus intrinsic reddening.

3. Method and Results

3.1. Model Absolute Magnitudes and Colors

We started with a model atmosphere grid for sdB stars initially developed by Brassard et al. (2010). The grid covers the ranges of $20{,}000 \leqslant T_{eff} \leqslant 50{,}000$ K in steps of 2000 K,

Table 3
Available Photometry

Name	G_{BP}	$(G_{BP} - G_{RP})$	V	$(B - V)$	y	$(b - y)$	g	$(g - r)$
PG 1047+003	13.213 ± 0.007 (a)	−0.518 ± 0.007	13.474 ± 0.004 (b)	−0.290 ± 0.003	13.484 ± 0.003 (c)	−0.133 ± 0.004	⋯	⋯
PG 0014+067	15.887 ± 0.007 (a)	−0.348 ± 0.008	16.089 ± 0.022 (d)	−0.197 ± 0.021	⋯	⋯	15.837 ± 0.004 (e)	−0.452 ± 0.006
PG 1219+534	12.936 ± 0.006 (a)	−0.548 ± 0.006	⋯	⋯	13.235 ± 0.029 (c)	−0.157 ± 0.017	⋯	⋯
Feige 48	13.235 ± 0.009 (a)	−0.438 ± 0.010	13.480 ± 0.026 (f)	−0.250 ± 0.013	13.446 ± 0.029 (c)	−0.116 ± 0.017	⋯	⋯
EC 05217−3914	15.296 ± 0.006 (a)	−0.490 ± 0.007	15.570 ± 0.020 (g)	−0.280 ± 0.020	15.550 ± 0.020 (c)	−0.110 ± 0.020	⋯	⋯
PG 1325+102	13.726 ± 0.008 (a)	−0.539 ± 0.009	14.019 ± 0.036 (d)	−0.285 ± 0.042	14.019 ± 0.012 (c)	−0.134 ± 0.002	13.710 ± 0.030 (e)	−0.550 ± 0.036
PG 0048+091	14.242 ± 0.005 (a)	0.230 ± 0.004	14.261 ± 0.020 (h)	0.193 ± 0.050	⋯	⋯	⋯	⋯
EC 20117−4014	12.406 ± 0.007 (a)	0.248 ± 0.007	12.470 ± 0.010 (i)	0.130 ± 0.010	⋯	⋯	⋯	⋯
PG 0911+456	14.435 ± 0.008 (a)	−0.521 ± 0.009	14.670 ± 0.022 (d)	−0.259 ± 0.031	⋯	⋯	14.378 ± 0.003 (e)	−0.521 ± 0.004
BAL 090100001	11.929 ± 0.007 (a)	−0.361 ± 0.009	12.100 ± 0.100 (j)	−0.240 ± 0.100	⋯	⋯	⋯	⋯
EC 09582−1137	15.017 ± 0.009 (a)	−0.458 ± 0.009	15.260 ± 0.050 (k)	−0.250 ± 0.030	⋯	⋯	⋯	⋯
KPD 1943+4058	14.752 ± 0.007 (a)	−0.320 ± 0.007	14.866 ± 0.027 (l)	−0.147 ± 0.017	14.906 ± 0.049 (c)	−0.024 ± 0.037	⋯	⋯
KPD 0629−0016	14.857 ± 0.007 (a)	−0.073 ± 0.008	⋯	⋯	15.014 ± 0.024 (c)	0.017 ± 0.023	⋯	⋯
KIC 02697388	15.127 ± 0.004 (a)	−0.274 ± 0.005	15.234 ± 0.020 (d)	−0.164 ± 0.030	⋯	⋯	15.003 ± 0.003 (e)	−0.416 ± 0.004
PG 1336−018	13.206 ± 0.019 (a)	−0.424 ± 0.024	⋯	⋯	13.450 ± 0.093 (c)	−0.107 ± 0.009	⋯	⋯
TIC 278659026	11.433 ± 0.008 (a)	−0.398 ± 0.009	11.570 ± 0.090 (m)	−0.220 ± 0.100	⋯	⋯	⋯	⋯

Note. (a) *Gaia* DR2, (b) Landolt (2009), (c) Wesemael et al. (1992), (d) Jester et al. (2005), (e) SDSS DR12, (f) Bern & Wramdemark (1973), (g) O'Donoghue et al. (2013), (h) Zacharias et al. (2013), (i) O'Donoghue et al. (1997), (j) Van Grootel (2008), (k) Kilkenny et al. (2006), (l) Allard et al. (1994), (m) Hog et al. (2000).

$4.6 \leqslant \log g \leqslant 6.4$ in steps of 0.2 dex, and $-4.0 \leqslant \log \mathrm{He/H} \leqslant 0.0$ in steps of 0.5 dex. These are NLTE model atmospheres computed with TLUSTY that include metal line blanketing using a representative metallicity ($C = 0.1$, $N = 1.0$, $O = 0.1$, $S = 1.0$, $Si = 0.2$, $Fe = 1.0 \times$ solar values). For each of these models, a synthetic spectrum was computed using SYNSPEC. The flux was then convolved with a bandpass. If the radius is known, this can be converted into an absolute magnitude for that bandpass. In a two-band system, a theoretical color index is then obtained by taking the difference between the two absolute magnitudes.

As given in Table 1, a typical seismic analysis provides, among other properties, estimates of the effective temperature, surface gravity, and total mass (and, hence, of the radius) of a pulsator. It does not constrain the atmospheric composition, in particular the helium-to-hydrogen ratio. However, we note that the absolute magnitudes and colors for these sdB models in the broad bandpasses of interest depend only slightly on the values of $\log \mathrm{He/H}$, especially for the subsolar values encountered in sdB stars (and see Table 2). In other words, we could have used pure H models to compute our absolute magnitudes. Still, to be somewhat more accurate, we adopted the values of $\log \mathrm{He/H}$ given in Table 2 for a given pulsator and used -2.0 in the two cases where spectroscopy has not provided an estimate.

Given a radius, we estimated the absolute magnitude for a given bandpass in 3D space (T_{eff}, $\log g$, $\log \mathrm{He/H}$) using parabolic interpolation. This has the advantage of leading naturally to an estimate of the uncertainty on the derived absolute magnitude given the uncertainties on the three basic parameters. A comparison with the apparent magnitude provides, of course, an estimate of the distance. A comparison of the theoretical color index with the observed value provides, in conjunction with an extinction model, a measure of the interstellar reddening. This leads to a revised estimate of the distance, corrected for reddening.

3.2. Distance and Reddening Index

The distance d to a star is derived through the standard equation

$$\log d = \frac{a - A_a - M_a + 5}{5}, \qquad (1)$$

where d is in parsec, a is the apparent magnitude, A_a is the absorption coefficient, and M_a is the absolute magnitude in a given photometric bandpass (a). The absorption coefficient is related to the usual interstellar reddening index $E(B - V)$ through the relation

$$A_a = K_a E(B - V), \qquad (2)$$

where K_a is a bandpass-dependent quantity that can be evaluated from a model of the interstellar extinction. We took the values of K_a from the work of Schlafly & Finkbeiner (2011) for the bandpasses of interest here (see column 4 in their Table 6). These are B and V (Landolt), b and y (Strömgren), and g and r (SDSS). In addition, using again the work of Schlafly & Finkbeiner (2011), we estimated the corresponding coefficient for the *Gaia* bandpasses G_{BP} (effective wavelength of 5320 Å) and G_{RP} (7970 Å) as $K_{\mathrm{BP}} = 2.81$ and $K_{\mathrm{RP}} = 1.56$.

The standard reddening index $E(B - V)$ can be estimated from the inferred reddening index in a two-band system (a and b)
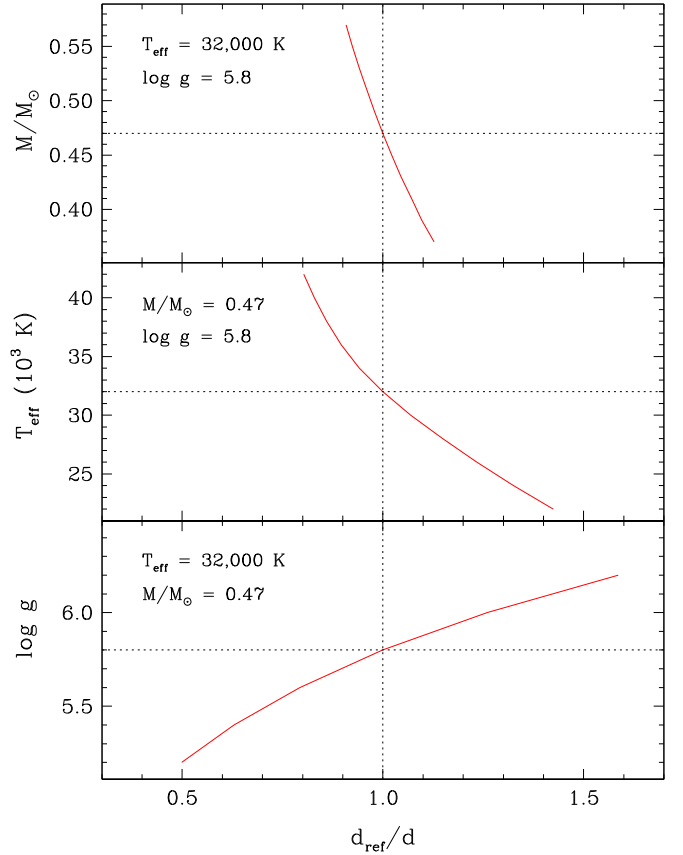

Figure 2. Variations of the inferred distance with respect to a reference model obtained by changing one seismic parameter in the range of interest for sdB stars, while keeping the other two fixed.

from the equation

$$E(B - V) = \frac{E(a - b)}{(K_a - K_b)}, \qquad (3)$$

in conjunction with

$$E(a - b) = (a - b) - (a - b)^0, \qquad (4)$$

where $(a - b)$ is the measured color index, and $(a - b)^0$ is the theoretical (unreddened) color index. The uncertainty in the derived distance to a pulsator is estimated, taking into account the uncertainties on the absolute magnitude M_a and theoretical color index $(a - b)^0$ (from parabolic interpolation in 3D space in our grids of models as well as a contribution from the uncertainty on the seismic radius), and the photometric errors on the observed magnitudes a and b. These errors are added in quadrature.

3.3. Distance and Seismic Parameters

In the current test, seismology provides input values of the effective temperature, surface gravity, and total mass. These are used to compute the absolute magnitude in a given bandpass in conjunction with an estimate of the helium-to-hydrogen number ratio taken from spectroscopy. The effects of the three seismic parameters on the distance are correlated, but it is still instructive to examine the effects of varying individually each of these parameters. This is best done by computing a difference of distance with respect to a reference model. From

Table 4
Comparison of Distances

Name	d(Gaia) (pc)	$d(G_{BP}G_{RP})$ (pc)	$d(BV)$ (pc)	$d(by)$ (pc)	$d(gr)$ (pc)
PG 1047+003	687 ± 37	609 ± 49	609 ± 42	613 ± 39	⋯
PG 0014+067	2794 ± 1037	1812 ± 277	1840 ± 306	⋯	1933 ± 268
PG 1219+534	549 ± 14	532 ± 35	⋯	534 ± 48	⋯
Feige 48	822 ± 27	769 ± 28	777 ± 40	784 ± 50	⋯
EC 05217−3914	1590 ± 108	1636 ± 154	1622 ± 86	1603 ± 182	⋯
PG 1325+102	862 ± 51	820 ± 23	808 ± 74	823 ± 19	827 ± 68
PG 0048+091	1058 ± 48	⋯	1197 ± 145[a]	⋯	⋯
EC 20117−4014	587 ± 13	⋯	653 ± 58[a]	⋯	⋯
PG 0911+456	1035 ± 75	958 ± 27	903 ± 63	⋯	941 ± 21
BAL 090100001	365.6 ± 8.6	386 ± 31	401 ± 100	⋯	⋯
EC 09582−1137	1553 ± 139	1376 ± 40	1372 ± 112	⋯	⋯
KPD 1943+4058	1274 ± 51	1242 ± 73	1152 ± 93	1159 ± 155	⋯
KPD 0629−0016	1011 ± 50	1022 ± 67	⋯	1134 ± 116	⋯
KIC 02697388[b]	1262 ± 64	1328 ± 76	1319 ± 133	⋯	1366 ± 76
KIC 02697388[c]	1262 ± 64	1295 ± 79	1288 ± 133	⋯	1332 ± 78
PG 1336−018	552 ± 19	541 ± 26	⋯	564 ± 41	⋯
TIC 278659026	203.7 ± 2.1	221 ± 21	210 ± 56	⋯	⋯

Notes.
[a] Distance not corrected for interstellar reddening.
[b] Seismic Model 1 from Charpinet et al. (2011).
[c] Seismic Model 2 from Charpinet et al. (2011).

Equation (1), one can compute a difference of distance

$$\log d - \log d_{ref} = \frac{M_{ref} - M}{5}, \qquad (5)$$

which depends only on the absolute magnitude and is valid for any bandpass.

We considered a representative sdB model specified by the values of $M/M_\odot = 0.47$, $T_{eff} = 32,000$ K, and $\log g = 5.8$ (and $\log$ He/H $= -2.0$). We next computed the ratio d_{ref}/d by varying successively one of the seismic parameters, keeping the other two fixed. The results are displayed in Figure 2, which shows how the distance depends on each of the parameters in the ranges of interest for sdB stars. That is, the ranges of $22,000 \lesssim T_{eff} \lesssim 42,000$ K, $5.2 \lesssim \log g \lesssim 6.2$, and $0.37 \lesssim M/M_\odot \lesssim 0.57$ (see, e.g., Heber 2016). Changing the mass by ± 0.1 $M_\odot$ about 0.47 $M_\odot$ implies a variation of about $\pm 10\%$ in distance, while changing the surface gravity by ± 0.5 dex about $\log g = 5.7$ implies a variation in distance some five times larger.

3.4. Results

The main results of this study are summarized in Table 4, where the Gaia distance (the inverse of the trigonometric parallax) for each pulsator is compared with seismic estimates derived from the method described above. Altogether, we obtained 40 values and 2 upper limits on the distance using seismic data and 4 different sources of photometry. Of central interest and significance here, all of these values overlap within 1σ with the parallax distances. We thus conclude that, within these uncertainties, *all* of the seismic models are compatible with Gaia parallaxes. They pass the test proposed at the outset.

The seismic distances are generally determined more precisely on the basis of Gaia photometry than in other photometric systems. This is a consequence of the superior quality of those photometric measurements compared to ground-based data (see Table 3). Also, the derived uncertainties

on the seismic distances, while generally larger than those on the Gaia distances, become comparable in several cases. Given that the seismic and parallax distances overlap within 1σ, we do not observe systematic effects either with the distance itself or with colors. We illustrate this with the four plots Figures 3(a) through (d). Note that these plots do not include PG 0014+067, which falls offscale with a Gaia distance of $d = 2794 \pm 1037$ pc. This is the farthest and faintest star in our sample, and is characterized by an atypically large uncertainty in its parallax measurement. We come back to that point below.

Our method also provides estimates of interstellar reddening, and this can be used to further test our results, although more loosely than in the case of the distance. The derived reddening index, $E(B - V)$, is listed in Table 5, to be compared with line-of-sight measurements, $E(B - V)_{mean}$, as given by Galactic dust reddening and extinction maps and using the Schlafly & Finkbeiner (2011) values.[11] To pass the test, the derived reddening index, which measures the extinction between Earth and the star, should be smaller than (or equal to) the total extinction along the line of sight measured by $E(B - V)_{mean}$. Table 5 indicates that this is indeed the case for the majority of our targets, except for three stars, PG 0014+067, Feige 48, and PG 1336−018, especially on the basis of Gaia photometry.

Given that these three objects are binary stars likely accompanied by faint main-sequence M stars, the most logical explanation for this "failure" is that the available photometry is sensitive enough to have picked intrinsic reddening along with interstellar reddening in these systems. There are hints that this is indeed the case; the $E(B - V)$ index inferred from $G_{BP}G_{RP}$ photometry is larger than those inferred from BV, by, and gr data (with caution due to the uncertainties). This behavior is what is expected in the presence of a faint red companion, given that the effective wavelength coverage in the $G_{BP}G_{RP}$

---

[11] No determination of interstellar reddening was possible on the basis of the polluted colors of the binary systems PG 0048+091 and EC 20117−4014.
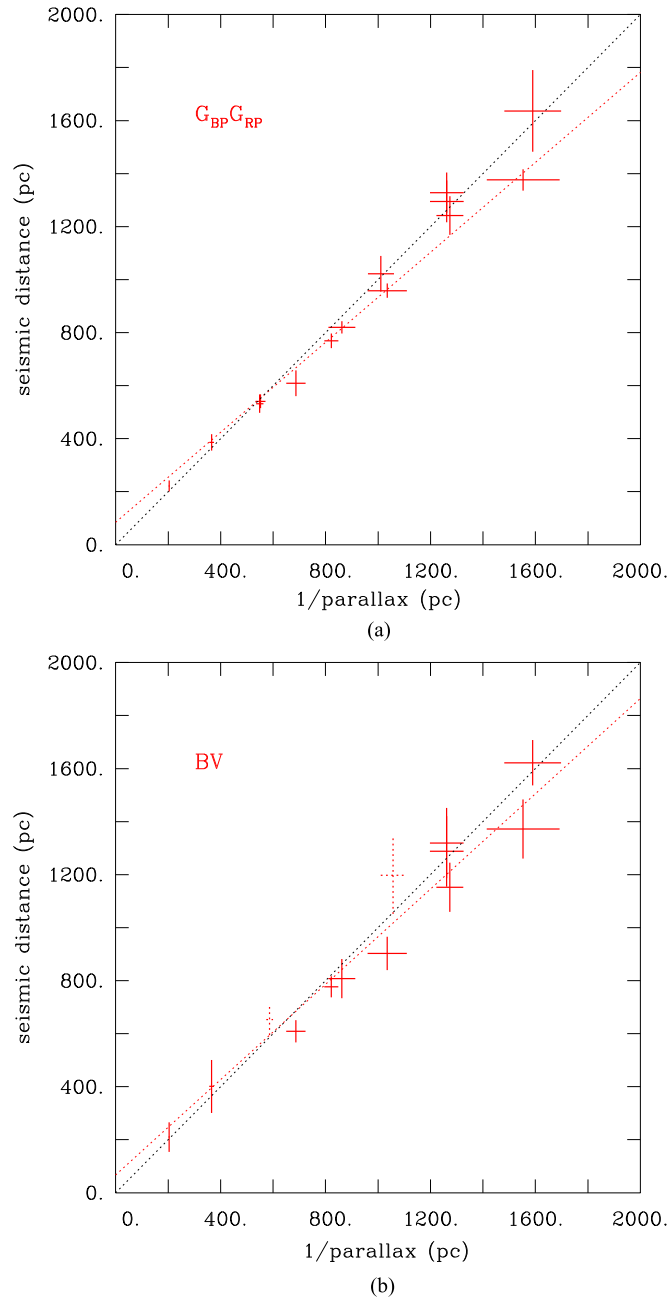
(a)

(b)

Figure 3. (a) Comparison of the *Gaia* distance (obtained by simply inverting the measured parallax) with the distance derived by combining a seismic model with a model atmosphere and measured *Gaia* magnitudes in the two bands G_{BP} and G_{RP}. The latter is corrected for the effects of interstellar reddening. The plot does not include PG 0014+067, which is an outlier due to the uncertainty in the *Gaia* distance of $d = 2794 \pm 1037$ pc (see the text). The black dotted line shows the 1:1 correspondence, while the red dotted line is a formal χ^2 fit giving a correlation coefficient of 0.984. (b) Similar to Figure 3(a), but based on the Johnson magnitudes *B* and *V*. The correlation coefficient is equal to 0.972. The seismic distances to two binary stars, PG 0048+091 and EC 20117−4014, are upper limits obtained under the assumption of no interstellar reddening. They are indicated by dotted crosses. (c) Similar to Figure 3(a), but based on the Strömgren magnitudes *b* and *y*. The correlation coefficient is equal to 0.980. (d) Similar to Figure 3(a), but based on the SDSS magnitudes *g* and *r*. The correlation coefficient is equal to 0.881.

system, 5320–7970 Å, is "redder" than those in the other systems (4329–5421 Å in *BV*, 4671–5479 Å in *by*, and 4717 −6165 Å in *gr*), and therefore more sensitive to such a presence. By construction, all of the reddening inferred in our approach is assumed to be due to interstellar absorption. In the case of the three binary systems of interest, this implies that too much reddening (sum of intrinsic and interstellar) has been used, meaning that the derived seismic distances in Table 4— for those three objects—are underestimated. Disregarding the

formal uncertainties for a moment, the seismic distances for PG 0014+067 and Feige 48 are indeed shorter than the parallax values. This prompted us to reassess our estimates of seismic distances for these three objects, given that we cannot infer interstellar reddening due to the presence of a red companion.

On the one hand, one can obtain an estimate of the upper limit on the seismic distance by neglecting reddening completely (as was done in Table 4 for PG 0048+091 and EC 20117−4014). The results are reported as *d*(max) in Table 6, to be compared again with the *Gaia* values. On the
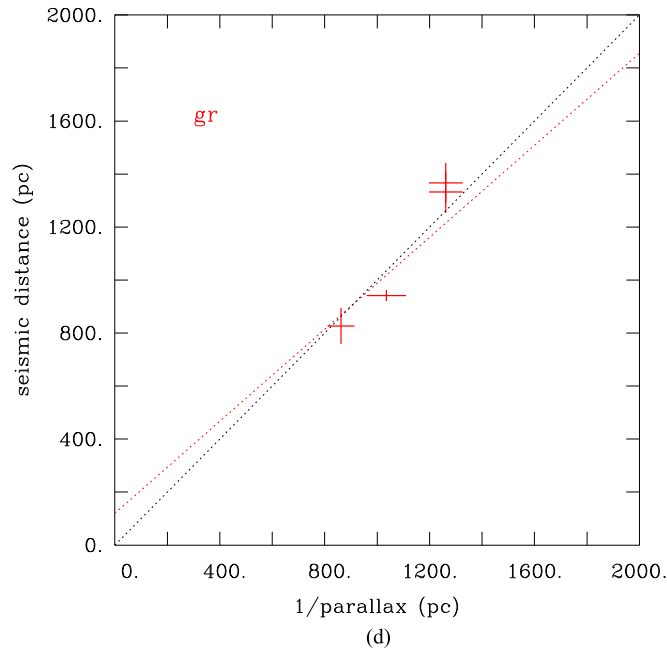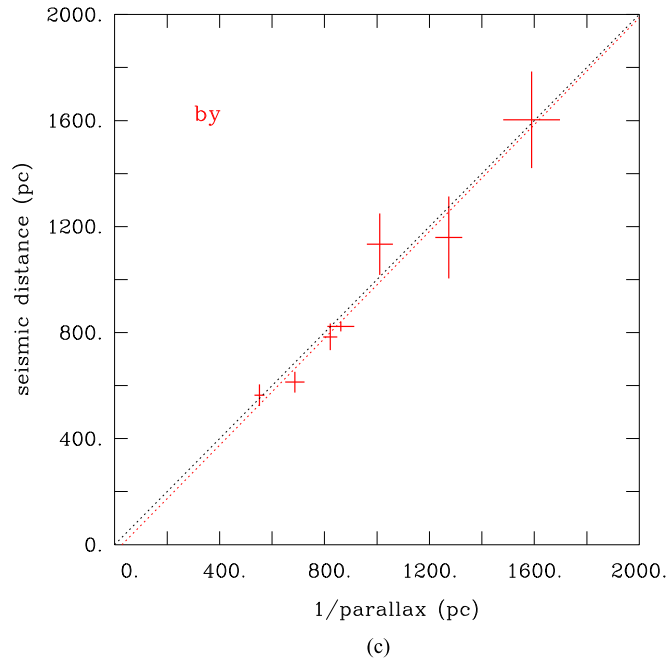
(c)

(d)

Figure 3. (Continued.)

other hand, a lower limit can be estimated by *assuming* maximum interstellar reddening, i.e., the values given by the index $E(B - V)_{mean}$ in Table 5. This is now given by d(min) in Table 6, where we compiled the results for all of the five binary systems in our sample using the available photometry. We also provided the results for the full range of possible values from d (min) to d(max) including the uncertainties. This range gives a conservative view of seismic distances for those five pulsators. These values clearly overlap with the *Gaia* distances.

A last point concerns the parallax measurement for PG 0014 +067. The *Gaia* uncertainty on that parallax is 37%, well above the values of 1%–9% which characterize the rest of the sample. From the detailed work of Bailer-Jones (2015), it is

known that inverting the parallax to obtain a distance in cases where the uncertainty is larger than ∼20% generally leads to significant underestimates of that distance. To investigate this point in the present case, we solved Equation (19) of Bailer-Jones in the context of her exponentially decreasing density galactic model. We adopted the representative exponential scale height of 450 pc as appropriate for sdB stars (Villeneuve et al. 1995). This provides a revised a posteriori estimate of the true distance. Our results are summarized in Table 7, which shows the value of the distance obtained by inverting the parallax (as we have done above) compared to the revised estimate. As expected, the revision leads to negligible changes for all our targets, except for PG 0014+067 whose distance to

Table 5
Inferred Interstellar Reddening

Name	$E(B-V)_{mean}$	$E(B-V)$ $(G_{BP}G_{RP})$	$E(B-V)$ (BV)	$E(B-V)$ (by)	$E(B-V)$ (gr)
PG 1047+003	0.037 ± 0.001	0.012 ± 0.018	0.003 ± 0.012	0.001 ± 0.010	⋯
PG 0014+067	0.033 ± 0.002	0.155 ± 0.030	0.114 ± 0.042	⋯	0.078 ± 0.019
PG 1219+534	0.017 ± 0.001	0.000 ± 0.014	⋯	0.000 ± 0.028	⋯
Feige 48	0.018 ± 0.002	0.046 ± 0.011	0.031 ± 0.018	0.015 ± 0.027	⋯
EC 05217-3914	0.022 ± 0.001	0.026 ± 0.020	0.024 ± 0.024	0.033 ± 0.035	⋯
PG 1325+102	0.027 ± 0.001	0.008 ± 0.008	0.018 ± 0.049	0.005 ± 0.003	0.000 ± 0.036
PG 0048+091	0.057 ± 0.001	⋯	⋯	⋯	⋯
EC 20117−4014	0.051 ± 0.001	⋯	⋯	⋯	⋯
PG 0911+456	0.010 ± 0.001	0.001 ± 0.009	0.032 ± 0.037	⋯	0.001 ± 0.005
BAL 090100001	0.092 ± 0.004	0.090 ± 0.021	0.031 ± 0.124	⋯	⋯
EC 09582−1137	0.057 ± 0.001	0.068 ± 0.010	0.057 ± 0.035	⋯	⋯
KPD 1943+4058	0.212 ± 0.005	0.124 ± 0.012	0.134 ± 0.023	0.147 ± 0.058	⋯
KPD 0629−0016	0.869 ± 0.009	0.300 ± 0.013	⋯	0.198 ± 0.038	⋯
KIC 02697388[a]	0.144 ± 0.013	0.130 ± 0.010	0.092 ± 0.038	⋯	0.066 ± 0.007
KIC 02697388[b]	0.144 ± 0.013	0.129 ± 0.011	0.091 ± 0.039	⋯	0.066 ± 0.008
PG 1336−018	0.046 ± 0.004	0.085 ± 0.020	⋯	0.038 ± 0.014	⋯
TIC 278659026	0.024 ± 0.001	0.004 ± 0.016	0.006 ± 0.121	⋯	⋯

Notes.
[a] Seismic Model 1 from Charpinet et al. (2011).
[b] Seismic Model 2 from Charpinet et al. (2011).

Table 6
Lower and Upper Limits on Seismic Distances for Binary Systems

Name	$d(Gaia)$ (pc)	$d(min)$ (pc)	$d(max)$ (pc)	Full Range (pc)	Bandpasses
PG 0014+067	2794 ± 1037	2121 ± 324	2213 ± 252	1797−2465	$G_{BP}G_{RP}$
PG 0014+067	2794 ± 1037	2037 ± 339	2123 ± 241	1698−2364	BV
PG 0014+067	2794 ± 1037	2069 ± 287	2175 ± 238	1782−2413	gr
Feige 48	822 ± 27	798 ± 29	817 ± 18	769−835	$G_{BP}G_{RP}$
Feige 48	822 ± 27	790 ± 41	808 ± 23	749−831	BV
PG 0048+091	1058 ± 48	1112 ± 173	1197 ± 145	939−1342	BV
EC 20117−4014	587 ± 13	611 ± 70	653 ± 58	541−711	BV
PG 1336−018	552 ± 19	569 ± 27	618 ± 13	542−631	$G_{BP}G_{RP}$

would now be 2156 pc instead of 2794 pc, a substantial reduction. Note that 2156 pc is in the middle of the ranges of seismic distance listed in Table 6.

4. Conclusion

The recent availability of high-accuracy parallaxes from *Gaia* DR2 has provided an opportunity to further test the seismic models for pulsating sdB stars that have been developed over the last several years. The latter are based on the forward modeling approach developed initially by Brassard et al. (2001), which uses parameterized static stellar models. Over the last decade, the method has been refined on the basis of more sophisticated models and optimization methods as described by Charpinet et al. (2016). A total of 16 pulsating sdBs have now been scrutinized through this seismic approach. Of particular interest are the four *g*-mode pulsators for which core probing was achieved. These are KPD 1943+4058, KPD 0629−0016, KIC 02697388, and TIC 278659026 (see Table 1 for the references).

Table 7
Revised *Gaia* Distances

Name	1/Parallax (pc)	Posterior Estimate (pc)
PG 1047+003	686.8	688.0
PG 0014+067	2793.6	2156.0
PG 1219+534	548.7	549.0
Feige 48	822.2	823.0
EC 05217−3914	1590.4	1580.0
PG 1325+102	861.8	863.0
PG 0048+091	1058.3	1050.0
EC 20117−4014	586.9	588.0
PG 0911+456	1035.0	1034.0
BAL 090100001	365.6	366.0
EC 09582−1137	1552.9	1536.0
KPD 1943+4058	1273.9	1273.0
KPD 0629−0016	1010.5	1010.0
KIC 02697388	1261.9	1260.0
PG 1336−018	552.0	553.0
TIC 278659026	203.7	204.0

The results of our investigation are summarized in Table 4, supplemented by Table 6 for the five binary systems in our sample, where the parallax distance is compared to values based on seismic estimates of the surface gravity, effective temperature, and total mass in conjunction with the available two-band photometry in four different systems. All of the values of the seismic distance are found to overlap with the *Gaia* distance within 1σ uncertainties. In addition, the inferred interstellar reddening is found to be consistent with line-of-sight extinction measurements as provided in Table 5 (taking into account intrinsic reddening in the binaries). This excellent agreement adds further credibility to the seismic models that have been calculated through the parameterized forward modeling approach developed for sdB stars. The method should find many more applications in the near future as *TESS* is now providing tens of new light curves for pulsating sdB stars, among many other outstanding data.

ORCID iDs

P. Bergeron ⬤ https://orcid.org/0000-0003-2368-345X
M. Latour ⬤ https://orcid.org/0000-0002-7547-6180

References

Alam, S., Alberati, F. D., Allende Prieto, C., et al. 2015, ApJS, 219, 12A, (SDSS DR12)
Allard, F., Wesemael, F., Fontaine, G., Bergeron, P., & Lamontagne, R. 1994, AJ, 107, 1565
Bailer-Jones, C. 2015, PASP, 127, 994
Baran, A., Pigulski, A., Koziel, D., et al. 2005, MNRAS, 360, 737
Bergeron, P., Saffer, R. A., & Liebert, J. 1992, ApJ, 394, 228
Bern, K., & Wramdemark, S. 1973, LowOB, 8, 1
Billères, M., & Fontaine, G. 2005, in ASP Conf. Ser. 334, 14th European Workshop on White Dwarfs, ed. D. Koester & S. Moehler (San Francisco, CA: ASP), 635
Brassard, P., Fontaine, G., Billères, M., et al. 2001, ApJ, 563, 1013
Brassard, P., Fontaine, G., Chayer, P., & Green, E. M. 2010, in AIP Conf. Proc. 1273, 17th European White Dwarf Workshop, ed. K. Werner & T. Rauch (Melville, NY: AIP), 259
Charpinet, S. 1999, PhD thesis, Univ. de Montréal
Charpinet, S., Brassard, P., Fontaine, G., et al. 2019, A&A, submitted
Charpinet, S., Fontaine, G., & Brassard, P. 2003, in NATO ASIB Proc. 105, White Dwarfs, ed. D. de Martino (Dordrecht: Kluwer), 69
Charpinet, S., Fontaine, G., Brassard, P., et al. 2005a, in ASP Conf. Ser. 334, 14th European Workshop on White Dwarfs, ed. D. Koester & S. Moehler (San Francisco, CA: ASP), 619
Charpinet, S., Fontaine, G., Brassard, P., et al. 2005b, A&A, 443, 251
Charpinet, S., Fontaine, G., Brassard, P., Chayer, P., & Green, E. M. 2006a, MmSAI, 77, 358
Charpinet, S., Fontaine, G., Brassard, P., Green, E. M., & Chayer, P. 2005c, A&A, 437, 575
Charpinet, S., Green, E. M., Baglin, A., et al. 2010, A&A, 516, L6
Charpinet, S., Silvotti, R., Bonanno, A., et al. 2006b, A&A, 459, 565
Charpinet, S., Van Grootel, V., Fontaine, G., et al. 2011, A&A, 530, A3
Charpinet, S., Van Grootel, V., Fontaine, G., et al. 2016, in XXIX IAU General Assembly 1, Astronomy in Focus, ed. P. Benvenuti (Cambridge: Cambridge Univ. Press), 581
Charpinet, S., Van Grootel, V., Reese, D., et al. 2008, A&A, 489, 377
Fontaine, G., Brassard, P., Charpinet, S., et al. 2003, ApJ, 597, 518
Fontaine, G., Brassard, P., Charpinet, S., et al. 2012, A&A, 539, A12
Gaia Collaboration, Babusiaux, C., van Leevwen, F., et al. 2018, A&A, 616, A10, (Gaia DR2)
Green, E. M., Fontaine, G., Hyde, E. A., For, B.-Q., & Chayer, P. 2008, in ASP Conf. Ser. 392, Hot Subdwarf Stars and Related Objects, ed. U. Heber, S. Jeffery, & R. Napiwotzki (San Francisco, CA: ASP), 75
Green, E. M., Fontaine, G., Reed., M. D., et al. 2003, ApJL, 583, L31
Heber, U. 2016, PASP, 128, 082001
Hog, E., Fabricius, C., Makarov, V. V., et al. 2000, A&A, 355, 27
Jester, S., Schneider, D. P., Richards, G. T., et al. 2005, AJ, 130, 873
Kilkenny, D., Koen, C., O'Donoghue, D., & Stobie, R. S. 1997, MNRAS, 285, 640
Kilkenny, D., O'Donoghue, D., Koen, C., Lynas-Gray, A. E., & van Wyk, F. 1998, MNRAS, 296, 329
Kilkenny, D., Stobie, R. S., O'Donoghue, D., et al. 2006, MNRAS, 367, 1693
Koen, C., O'Donoghue, D., Kilkenny, D., & Pollaco, D. L. 2004, NewAR, 9, 565
Koen, C., O'Donoghue, D., Kilkenny, D., Stobie, R. S., & Saffer, R. A. 1999, MNRAS, 306, 213
Landolt, A. U. 2009, AJ, 137, 4186
Latour, M., Fontaine, G., & Green, E. 2014a, in ASP Conf. Ser. 481, 6th Conf. Hot Subdwarf Stars and Related Objects, ed. V. Van Grootel et al. (San Francisco, CA: ASP), 91
Latour, M., Fontaine, G., Green, E. M., Brassard, P., & Chayer, P. 2014b, ApJ, 788, 65
Németh, P., Kawka, A., & Vennes, S. 2012, MNRAS, 427, 2180
O'Donoghue, D., Kilkenny, D., Koen, C., et al. 2013, MNRAS, 431, 240
O'Donoghue, D., Lynas-Gray, A. E., Kilkenny, D., Stobie, R. S., & Koen, C. 1997, MNRAS, 285, 657
Østensen, R. H., Oreiro, R., Solheim, J.-E., et al. 2010, A&A, 513, A6
Otani, T., Oswalt, T. D., Lynas-Gray, A. E., et al. 2018, ApJ, 859, 1450
O'Toole, S. J., Heber, U., & Benjamin, R. A. 2004, A&A, 422, 1053
Randall, S. K., Fontaine, G., Charpinet, S., et al. 2006a, ApJ, 648, 637
Randall, S. K., Fontaine, G., Green, E. M., et al. 2006b, ApJ, 643, 1198
Randall, S. K., Green, E. M., Fontaine, G., et al. 2006c, ApJ, 645, 1464
Randall, S. K., Green, E. M., Van Grootel, V., et al. 2007, A&A, 476, 1317
Randall, S. K., Van Grootel, V., Fontaine, G., Charpinet, S., & Brassard, P. 2009, A&A, 507, 911
Reed, M. D., Telting, J. H., Ketzer, L., et al. 2019, MNRAS, 483, 2282
Schlafly, E. F., & Finkbeiner, D. P. 2011, ApJ, 737, 103
Schuh, S., Huber, J., Dreizler, S., et al. 2006, A&A, 445, 31
Van Grootel, V. 2008, PhD thesis, Univ. de Toulouse
Van Grootel, V., Charpinet, S., Brassard, P., Fontaine, G., & Green, E. M. 2013, A&A, 553, A97
Van Grootel, V., Charpinet, S., Fontaine, G., et al. 2008, A&A, 488, 685
Van Grootel, V., Charpinet, S., Fontaine, G., et al. 2010a, ApJL, 718, L97
Van Grootel, V., Charpinet, S., Fontaine, G., Green, E. M., & Brassard, P. 2010b, A&A, 524, 63
Villeneuve, B., Wesemael, F., Fontaine, G., Carignan, C., & Green, R. F. 1995, ApJ, 446, 646
Wesemael, F., Fontaine, G., Bergeron, P., Lamontagne, R., & Green, R. F. 1992, AJ, 104, 203
Zacharias, N., Finch, C. T., Girard, T. M., et al. 2013, AJ, 145, 44